A SU-8-Based Fully Integrated Biocompatible Inductively Powered Wireless Neurostimulator

Sung-Hoon Cho, Ning Xue, *Student Member, IEEE*, Lawrence Cauller, Will Rosellini, and Jeong-Bong Lee, *Senior Member, IEEE*

***Abstract*—A fully integrated minimally invasive compact polymer-based wireless neurostimulator was designed, fabricated, and characterized both in open air and *in vivo*. The neurostimulator ($3.1 \times 1.6 \times 0.3$ mm) consists of a planar spiral coil for wireless power supply through inductive coupling, two Schottky diodes for full-wave rectification, an application-specific integrated circuit neurostimulator circuit chip for stimulus spike signal generation, and two biphasic platinum–iridium (PtIr) stimulation electrodes. The device is fully integrated and completely embedded in biocompatible SU-8 packaging. For *in vivo* testing, the wireless neurostimulator was implanted subcutaneously in a rat hind limb. At the coupling power of 21 dBm (125 mW) at 394-MHz resonant frequency, stable and robust cortical responses during extended periods of wireless stimulation were recorded. [2012-0085]**

***Index Terms*—Implantable, inductive coupling, neurostimulator, SU-8, wireless.**

I. Introduction

NERVE CELLS and their respective networks play important roles in the sensory and motor abilities of a human body. Destruction of nerve cell networks resulting from diseases or injuries may cause permanent loss of voluntary motor or sensation functions. Detection and stimulation of neural activities using microelectromechanical systems (MEMS)-based microprobes have been one of the primary research areas in the field of neural engineering for over 25 years. These microprobes have been designed to be implanted to act as an interface between neurons and electronics for the stable detection of neural spike signals or for efficient stimulation of neurons and their fibers. Neural spike signals can be used to control the movement of prosthetic limbs or other assistive robotics [1]. Meanwhile, neural stimulation can mediate sensory feedback from sensors such as tactile, pressure, and force sensors to restore natural sensations with prosthetic limbs [2].

Electrical stimulation of peripheral nerves is widely employed to treat regional neuropathic pains. Weiner and Reed reported the treatment of occipital neuralgia by inserting electrodes in the vicinity of occipital nerves [3]. Slavin and Burchiel reported the usage of this technique in both occipital and trigeminal areas [4]. The same technique was also used to treat inguinal pain, low back pain and sacroiliac pain, and postherpetic pain [5]–[7]. These methods involve delicate surgical procedures to implant electrodes with a bundle of long lead wires to connect to bulky controllers. Such methods can cause risk of infection, long-term patient trauma or nerve damage, and reduction of functional reliability. Also, it is often related to problems with the wiring or physical motion of implanted electrodes.

To avoid these issues, wireless operation of the implanted neural stimulation devices is highly desirable. In order to realize such a wireless neural stimulator, it should have an onboard power source and also contain a circuitry to generate a specific neural stimulus electrical signal. A battery as the onboard power source can be a candidate for such a wireless operation, but its use is limited due to its limited lifespan and potential risk of leakage of toxic material inside the battery. Wireless power transmission from the outside of the body to the implanted devices in the body would be an alternate method. The transcutaneous power transfer can be accomplished by utilizing electromagnetic induction between two magnetically coupled coils: a transmitter coil located outside of the body and a receiver coil implanted in the body. Inductively coupled implantable devices have been utilized to restore paralyzed limb function, improve bladder voiding, measure intraocular pressure and blood pressure, and record peripheral neural activities [8]–[13].

There have been several investigations on the wireless biomedical implantable neurostimulator and neurorecorder. Table I shows comparison among the previously developed MEMS-based wireless neural implants [13]–[16]. The reported wireless neural implants in Table I were board level packaged and therefore relatively bulky for selective peripheral nerve stimulation applications. Furthermore, biocompatibility is one of the most critical issues for the development of any implantable devices. The device should be made of biocompatible materials and thoroughly sterilized so that the device does

Manuscript received April 4, 2012; revised August 7, 2012; accepted September 12, 2012. Date of publication October 22, 2012; date of current version January 30, 2013. This work was supported in part by the Texas Emerging Technology Fund and in part by a National Institutes of Health (NIH), Small Business Technology Transfer (STTR) program. Subject Editor S. Shoji.

S.-H. Cho was with the Micro–Nano Devices and Systems Laboratory, Department of Electrical Engineering, The University of Texas at Dallas, Richardson, TX 75080 USA. He is now with Samsung Electronics Company, Ltd., Seoul 137-857, Korea (e-mail: sh2010.cho@samsung.com).

N. Xue is with the Micro–Nano Devices and Systems Laboratory, Department of Electrical Engineering, The University of Texas at Dallas, Richardson, TX 75080 USA, and also with Agiltron, Inc., Woburn, MA 01801 USA (e-mail: nxx083000@utdallas.edu).

L. Cauller, retired, was with the Neuroscience Program, School of Behavioral and Brain Sciences, The University of Texas at Dallas, Richardson, TX 75080 USA (e-mail: cauller@utdallas.edu).

W. Rosellini is with the School of Behavioral and Brain Sciences, The University of Texas at Dallas, Richardson, TX 75080 USA, and also with Microtransponder, Inc., Dallas, TX 75230 USA (e-mail: wmr013000@utdallas.edu).

J.-B. Lee is with the Department of Electrical Engineering, The University of Texas at Dallas, Richardson, TX 75080 USA (e-mail: jblee@utdallas.edu).

Color versions of one or more of the figures in this paper are available online at http://ieeexplore.ieee.org.

Digital Object Identifier 10.1109/JMEMS.2012.2221155

TABLE I
PREVIOUSLY REPORTED WIRELESS NEUROSTIMULATOR AND RECORDER IMPLANTS

	Device Dimensions	Operating frequency	Power consumption	Application
T. Akin et al. (1998)	5 × 8 × 2 mm	2 MHz	90 mW	Peripheral neural recording
C.W. Peng et al. (2004)	3 cm diameter	2 MHz	30 mW	Neuromuscular control
L. Theogarajan et al. (2006)	12 × 31 mm	125 MHz	2 mW	Retinal prototype
M. Ghovanloo et al. (2007)	19 × 14 × 6 mm	5/10 MHz	50 mW	Chronic pain management

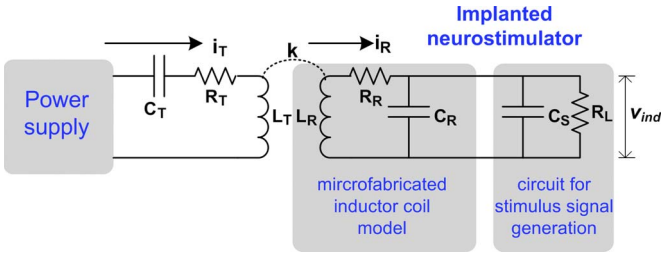

Fig. 1. Schematic of wireless inductive coupling system, including power supply system and implanted neurostimulator.

not damage surrounding tissues and does not cause biofouling during long-term exposure to the physiological environment. Most of the biomedical implantable devices use silicon as the basic materials. Silicon has been demonstrated as a least biocompatible material with higher density of adherent cells in the biofouling test. By contrast, Voskerician *et al.* found that gold, silicon nitride, silicon dioxide, and SU-8 are less prone to biofouling [17]. Also, from our previous experiment, we found that SU-8-based implant is biocompatible and there was no apparent sign of tissue damage or inflammatory reaction for over 51-week *in vivo* test, and successful recording of spike signals using wired SU-8-based microprobe was achieved [18]. In this paper, we developed a SU-8-based fully integrated minimally invasive compact wireless implantable neurostimulator using MEMS technology [19]. Our device is a factor of ten times smaller than what were reported previously. It is powered without implanted batteries or wires by receiving electromagnetic power from a transmitter coil placed on the surface of the overlying skin.

II. DESIGN AND THEORY

A. Inductive Coupling Power Transfer System

The implanted depth for effective device operation is limited by the amount of power delivered to the implanted device. Thus, for certain reliable working distance, the efficiency of the power transfer between the power transmitter coil and the receiver coil should be maximized. Fig. 1 shows the schematic of the inductive coupling system for power transfer from external circuit to wireless implanted neurostimulator.

Theoretically, when the inductive coupling is small $(R_T R_R \ll \omega k^2 L_T L_R)$, the induced voltage (v_{ind}) at implanted neurostimulator is given by [20], [21]

$$|v_{\text{ind}}| = \frac{\omega \cdot k \cdot \sqrt{L_T L_R} \cdot i_T}{\sqrt{\left[\frac{\omega L_R}{R_L} + \omega R_R (C_R + C_S)\right]^2 + \left[1 - \omega^2 L_R (C_R + C_S) + \frac{R_R}{R_L}\right]^2}} \quad (1)$$

where ω is the operating angular frequency, k is the coupling coefficient between the transmitter and the receiver coils, i_T and i_R are the current flow through the transmitter coil and receiver coil, respectively, L_T and L_R represent the transmitter and the receiver coil inductances, respectively, C_T is the capacitance of the capacitor connecting the transmitter coil serially, C_R is the parasitic capacitance of the receiver coil, C_S is the total capacitance of the circuit for stimulus signal generation, R_T is the resistance of the transmitter coil, and R_R and R_L denote the series resistance of the receiver coil and the load of the transponder chip, respectively.

At resonant frequency $(f_{\text{work}} = f_{\text{resT}} = f_{\text{resR}})$, induced voltage reaches maximum value, and (1) can be simplified to

$$|v_{\text{ind}}| = \frac{\omega \cdot k \cdot \sqrt{L_T L_R} \cdot i_T}{\frac{\omega L_R}{R_L} + \frac{R_R}{\omega L_R}} = \omega \cdot k \cdot \sqrt{L_T L_R} \cdot i_T \cdot Q \quad (2)$$

where $Q = (\omega L_R / R_L + R_R / \omega L_R)^{-1}$ is the quality factor of the implanted neurostimulator circuit. From (2), we know that higher induced voltage at the implant can be obtained by higher coupling coefficient, higher Q factor, and higher inductance of the receiver coil.

The coupling coefficient between two coils depends on various factors such as coils' geometries, distance, and alignment between the coils [20]. Due to physiological constraints of our target application of peripheral nerve stimulation, the diameter of the receiver coil was decided to be 1 mm. Its desirable working distance was subcutaneous level of 5 mm. The Q factor of the receiver system is one of the most important factors for the maximum efficiency of power delivery. In this paper, the input port of the load of the transponder chip consists of two diodes and two smooth capacitors, which has large input resistance, meaning that R_L is large. The Q factor of the receiver system can be simplified to be

$$Q = \frac{\omega L_R}{R_R}. \quad (3)$$

To improve the Q factor, the inductance of the receiver coil should be maximized. Meanwhile, it is required to reduce the series resistance which depends on skin depth and proximity effect, as well as conductor's resistivity and geometry. In a given space, although inductance increases as the number of turns of the coil increases, it makes conductor traces narrower resulting in higher series resistance and higher parasitic capacitance. Therefore, it is necessary to find optimized geometrical parameters of the receiver coil such as width, pitch distance, and thickness of the conductor traces. The thickness of the inductor was chosen to be 10 μm, which is 2.5 times the skin depth at 400 MHz. Beyond 10 μm thick, resistance would not decrease significantly.

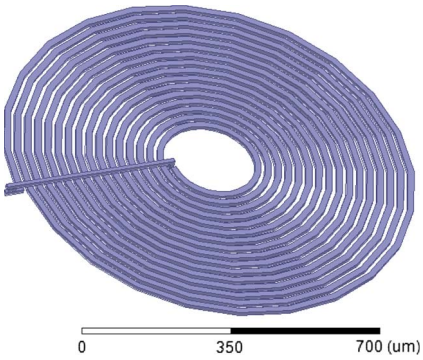

Fig. 2. HFSS model for planar circular coil.

TABLE II
Q FACTOR COMPARISON AMONG THREE SIZES OF INDUCTOR COILS

Turns	Trace width (μm)	Gap between two traces (μm)	Q factor
26	5	10	32
20 (for this design)	10	10	29
16	15	10	24

Extensive simulations were performed to find out optimal coil geometry using HFSS (Ansoft Corporation). Fig. 2 shows the planar circular coil model used in HFSS to extract the Q factor of the receiver. Table II lists a comparison of the Q factor among three different sizes of coils, with identical outer diameter of 1 mm and inner diameter of 0.2 mm.

From Table II, 5-μm-wide trace can get higher Q because of increased inductance. In contrast, the coil trace with 15-μm width has the smallest Q factor. However, fabrication of narrow coil trace with higher aspect ratio is difficult to achieve. Furthermore, the Q factor with 10-μm-wide trace coil is quite close to that of 5-μm-wide trace coil. Therefore, in this work, a planar circular inductor was designed to have 1-mm diameter, 20 turns, 10-μm-width coil trace, and 20-μm pitch distance.

B. Design of Microneurostimulator

Switched-capacitor stimulation (SCS) method has been proved to be an efficient method to stimulate peripheral nerves [22]. Also, it involves relatively simple electric circuit with minimal number of components. Conventional neural stimulation methods such as voltage-controlled stimulation and current-controlled stimulation need complex circuit to control precisely timed pulses whose amplitude is regulated to be constant [23]. In contrast, SCS needs only a charge-up capacitor and a switching circuit. Consequently, the SCS application-specific integrated circuit (ASIC) chip can be realized with small size. Platinum–iridium was used as electrode material. It is one of the most commonly used materials in electrical nerve stimulation due to its high charge-carrier capacity $(300-350\ \mu\mathrm{C/cm^2})$ and mechanical robustness [24].

Fig. 3 shows the schematics of our MEMS-based wireless battery-free compact neurostimulator. The overall size is $3.1 \times 1.5 \times 0.3$ mm. It consists of a planar circular inductor as a power coupling element, two Schottky diodes for full-wave rectification, an ASIC neurostimulator circuit chip for stimulus signal generation, and biphasic platinum–iridium (PtIr) stimulation electrodes. Due to its biocompatible requirement,

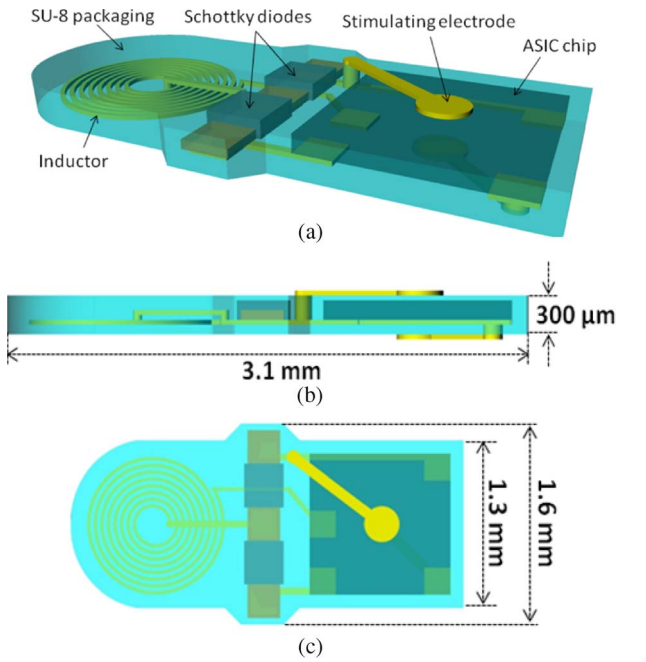

Fig. 3. Schematic diagrams of SU-8-packaged wireless neurostimulator: (a) three-dimensional view showing a receiver coil, two rectifying Schottky diodes, a stimulating ASIC chip, and biphasic stimulating electrodes; (b) side view; and (c) top view of the device.

biocompatible SU-8 [18] was used as a packaging material as well as all interlevel insulative layers.

The full-wave rectifier located right next to the receiver coil was composed of two commercially available Schottky diodes $(830 \times 300 \times 95\ \mu\mathrm{m})$ (M2X8554, Metelics, Inc.). Rectified output signals from the rectification diodes are transferred to the input pads of the ASIC chip $(1 \times 1 \times 0.15$ mm). The ASIC neurostimulator chip controls charge stimuli by employing a bistable switch to oscillate between the charging phase that builds up a charge on the stimulus capacitor (1.5 nF) and the discharge phase that is triggered when the charge reaches the desired stimulation voltage by closing the switch to discharge the capacitor through the stimulus electrodes. Stimulus signals from the ASIC output is delivered to the 1-mm-diameter PtIr stimulating electrodes which are positioned at both the top and bottom surfaces of the device.

Fig. 4 shows the equivalent circuit model of the designed wireless neurostimulator. The junction capacitance (0.2 pF) of the Schottky diodes was used for tuning the resonant frequency of the receiver coil rather than using microfabricated capacitors. Along with the smoothing capacitors (47 pF), the total capacitance of the full-wave rectification circuit applied in frequency tuning was 0.38 pF. The calculated resonant frequency of the receiver coil was 510 MHz. However, if parasitic capacitance was considered, the actual resonant frequency of the receiver should be lower and should get close to the target operating frequency of 400 MHz.

III. FABRICATION

The designed wireless neurostimulator was fabricated by SU-8-based surface micromachining technique. The fabrication process flow is shown in Fig. 5. The fabrication was started

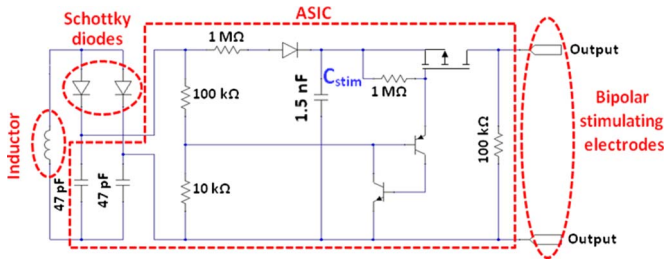

Fig. 4. Equivalent circuit model of the wireless neurostimulator showing switching circuit and stimulating capacitor C_{stim} in the ASIC chip.

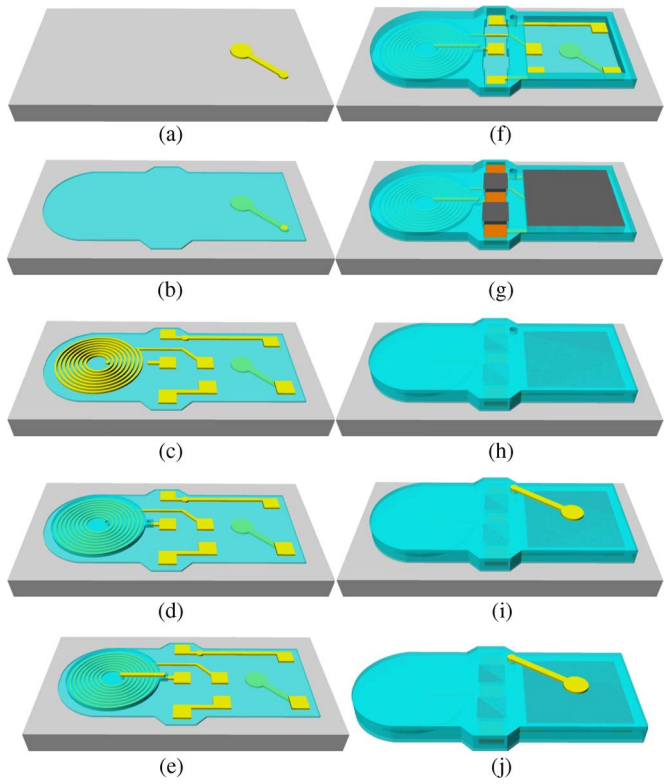

Fig. 5. Fabrication process flow of the wireless neurostimulator: (a) Patterning of the bottom gold electrode; (b) formation of the base layer of the SU-8 socket platform; (c) conductor traces of the spiral inductor and the contact pads; (d) SU-8 insulation on top of the spiral inductor with via holes; (e) conductor bridge over the spiral inductor; (f) 156-μm-thick SU-8 sockets; (g) diodes and ASIC chip packaging into the sockets; (h) 100-μm-thick SU-8 protection layer with the output via hole; (i) patterning of the top gold stimulating electrode; and (j) device completely released from the substrate.

with deposition of Cr (250 Å) and Au (1000 Å) electroplating seed layer on the 3-in Pyrex substrate by using thermal evaporator. Then, 15-μm-thick SPR-220 photoresist (Rohm and Haas, Midland, MI) was created by UV lithography as electroplating mold. Ten-micrometer-thick gold was electroplated as the output bipolar pad of ASIC chip [Fig. 5(a)]. After removal of the Cr/Au seed layer, OmniCoat (MicroChem Corporation, Newton, MA) was coated to enhance adhesion between the Pyrex substrate and the next layer. A 10-μm-thick SU-8-2010 (MicroChem Corporation, Newton, MA) layer was patterned, exposing a via hole leading to the bottom gold electrode. Next, a 100-nm-thick gold electroplating seed layer was deposited by using dc sputtering, followed by creating a 15-μm-thick electroplating mold with SPR-220 photoresist. Then, 10-μm-thick conductor traces of the spiral inductor and contact pads of the socket were built by gold electroplating [Fig. 5(c)]. Next, 15-μm-thick SU-8 was formed as the intermediate insulation layer over the conductor traces [Fig. 5(d)]. After filling up both via holes by electroplating, a 10-μm-thick conductor bridge over the spiral inductor was created on top of the SU-8 layer by gold electroplating [Fig. 5(e)]. A 156-μm-deep SU-8 socket structure was then patterned by SU-8-2075 in order to make sure that both the diodes and the ASIC are completely enclosed by SU-8 socket [Fig. 5(f)]. The fabricated SU-8 socket platform with coils and pad is shown in Fig. 6.

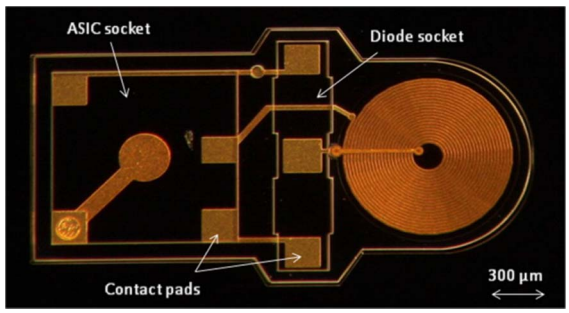

Fig. 6. Fabricated SU-8 socket platform with ASIC and diode sockets, contact pads on the bottom floor of the socket, and embedded spiral inductor.

After the completion of the SU-8 socket platform fabrication, integration process was performed manually under a stereo microscope. A small amount of biocompatible conductive epoxy was applied to the contact pads of the sockets. Then, the ASIC chip and diodes were slid into the sockets with their contact pads side down as shown in Fig. 5(g). Because solvent inside the biocompatible conductive epoxy can affect the subsequent SU-8 process, it should be completely evaporated. Thus, the sample was cured in a 95-°C convection oven for 5 h to thoroughly evaporate the solvent of the conductive epoxy. Subsequently, the device was thoroughly sealed by 100-μm-thick SU-8, and one of the via holes were created through the SU-8 sealing on the purpose of output pad connection as shown in Fig. 5(h). During the SU-8 sealing process, air bubbles are created on the SU-8 sealing due to uneven surface of the sample caused by the air gap between the socket wall and the off-chip components. These air bubbles sometimes make the metal contacts or traces be exposed to the air, causing device failure in the physiological environment. In order to avoid this issue, SU-8 should be spin coated with lower ramping speed. Also, longer planarization process before SU-8 curing was carried out. The output via hole was then filled by gold electroplating, followed by creating the top stimulating electrode by the same electroplating process [Fig. 5(i)]. The fabricated devices were then completely released from the Pyrex wafer by using buffered-oxide-etch etchant for about 24 h [Fig. 5(j)].

Finally, biocompatible conductive epoxy was applied to attach 1-mm-diameter PtIr stimulating electrodes on the electroplated gold electrodes at both the top and the bottom surfaces, and also, biocompatible conductive epoxy was used to completely fill up the output via for connection between the PtIr stimulating electrodes and the output of the ASIC chip. Fig. 7(a) shows the successfully fabricated device after integration

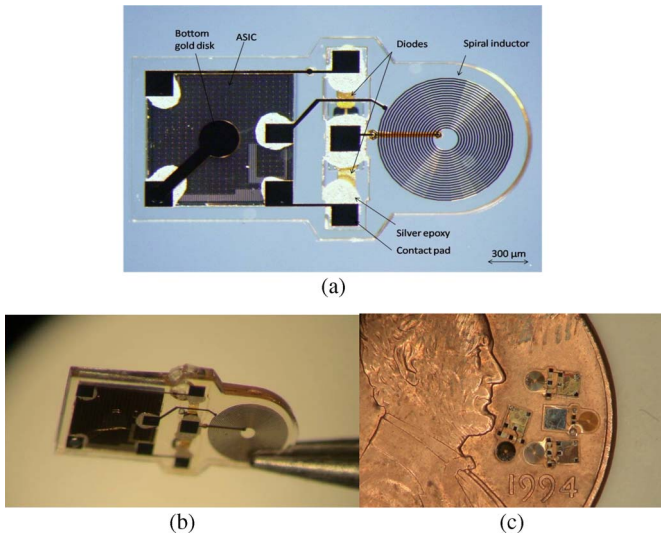

Fig. 7. Photomicrographs of the fabricated wireless neurostimulator: (a) Conductive epoxy was applied to the socket contact pads, and a couple of Schottky diodes and the ASIC chip were cemented; (b) the device was completely sealed by SU-8 and released from the substrate; and (c) released devices are on the one-cent coin.

process, and Fig. 7(b) and (c) shows the released device from the substrate.

IV. Characterization

A. Open-Air Test

Prior to *in vivo* study, open-air tests were carried out at different separation distances between the wireless simulator and the RF power coil. In order to measure the output stimulus from the PtIr stimulating electrodes, copper wires were clamped on both electrodes. The wired device was held to the RF power coil (operating frequency of 394 MHz) coaxially at different distances as shown in Fig. 8(a). The switched-capacitor-based stimulus voltage was detected by an oscilloscope. Fig. 8(b) shows measured stimulus output at different separation distances from the RF power coil. As it can be seen, the maximum peak value of the stimulus output decreases as the separation distance increases due to decrease in induced voltage in the receiver coil. The measured maximum peak voltage was approximately 6.5 V with 1-W power at 1-mm distance. Fig. 8(c) also showed that the wireless stimuli remained stable at repetition rates of up to 100 stimuli/s.

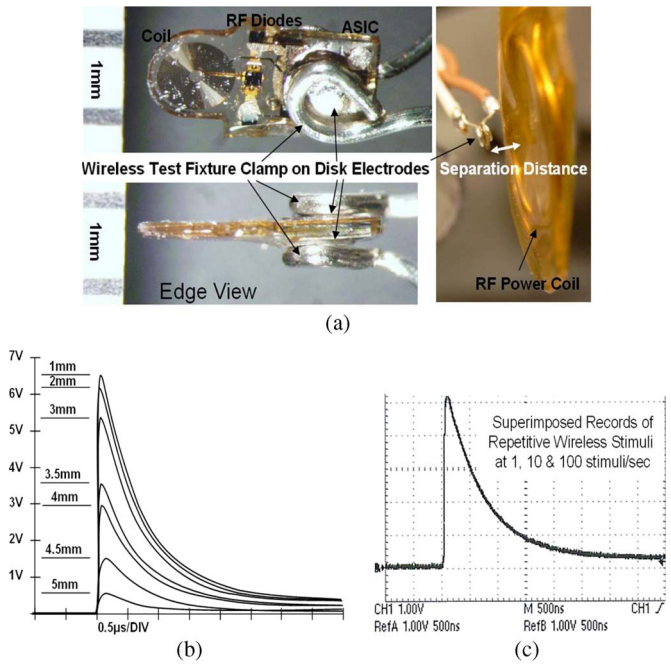

Fig. 8. Test fixture to evaluate the open-air wireless performance of the fully assembled microstimulator: (a) Test setup; (b) wireless stimulus decreasing with the increase of the separation distance between two coils at RF power of 1 W at 394 MHz; (c) wireless stimulus amplitude was stable at rates of up to 100 stimuli/s.

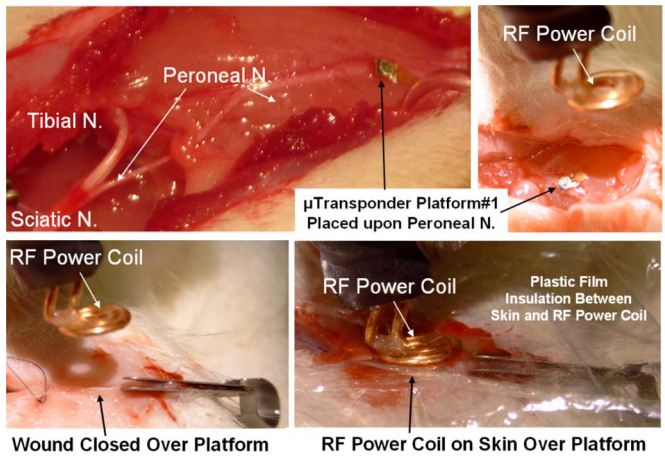

Fig. 9. Acute surgical rat preparation for subcutaneous placement of microstimulator implants to record the cortical response to wireless stimulation of the hind limb.

B. In Vivo Test

Subsequently, the fabricated neurostimulator was placed subcutaneously upon the peroneal nerve of a rat. The cortical responses to wireless stimulation powered by an external RF coil applied above the skin over the implant were recorded by wired head cap. Fig. 9 shows the subcutaneous placement of a wireless neurostimulator and the external RF power coil on the skin overlying the implant. One end of the SU-8-packaged neurostimulator is designed as round corner, and it has a slender shape (1.6 mm by 3.1 mm), which facilitates the insertion of device to tissue with small surgical cut ($\sim$2 mm). No tissue damage or device breakage was observed during the surgical implantation.

As can be seen in Fig. 10, increasing wireless stimulation intensity by increasing the external RF power up to 1 W (at 394 MHz) resulted in an increase in the amplitude of the evoked cortical responses. For comparison, the response amplitudes at this cortical site evoked by "transcutaneous-electrical-nerve-stimulation-like" stimulation of the plantar hindpaw ($\pm$2-mA constant current biphasic stimuli $\times$ 0.2 ms; Neuro Data PG4000 Digital Stimulator with Bak Electronics, Inc. BSI-2 Isolator) corresponded to response amplitudes evoked by wireless stimulation at an applied RF power level of 125 mW.

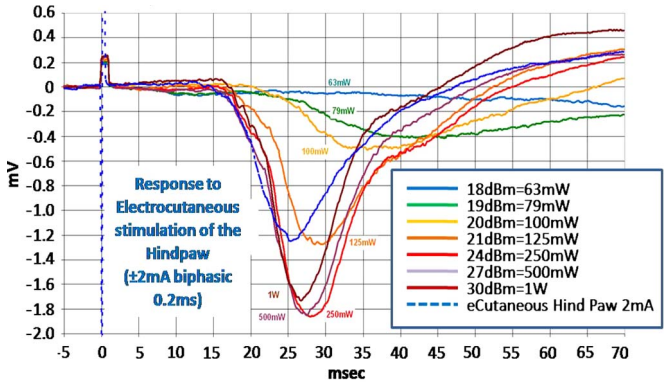

Fig. 10. Robust cortical responses evoked by wireless stimulation across a range of RF power levels.

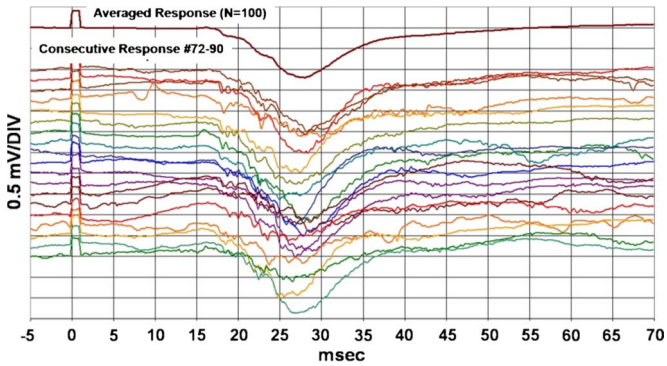

Fig. 11. Cortical responses to wireless subcutaneous stimulation over the peroneal nerve in the rat hind limb with evoked unit activity apparent in single-trial recordings at 125-mW input power.

Examples of the stable and robust cortical responses recorded during extended periods of wireless stimulation are shown in Fig. 11 where consecutive responses reliably approximated the averaged response with unitary spikes apparent on single-trial responses consistently activated during each evoked potential at 125-mW input power.

V. Conclusion

A fully integrated minimally invasive compact biocompatible SU-8-packaged wireless neurostimulator has been designed, fabricated, and characterized. The device consists of a receiver coil, two Schottky diodes, ASIC chip, and biphasic PtIr stimulating electrodes. The overall size of the fabricated device is $3.1 \times 1.5 \times 0.3$ mm, which is at least ten times smaller than that of the previously reported wireless implantable device. After open-air tests, the fabricated wireless neurostimulator was implanted subcutaneously in a rat hind limb, and stable and robust cortical responses during extended periods of wireless stimulation with as low as 21-dBm (125-mW) RF power at 394 MHz were recorded. This MEMS-based compact wireless neurostimulator has a great potential to be used for chronic pain management application by deploying multiple numbers of wireless stimulator subcutaneously in the region of interest.

Acknowledgment

The authors would like to thank the members of the Micro/Nano Devices and Systems Laboratory, The University of Texas at Dallas (UT Dallas), and the staff of the Cleanroom Research Laboratory, UT Dallas, for their help on device fabrication.

References

[1] D. J. Edell, "A peripheral nerve information transducer for amputees: Long-term multichannel recordings from rabbit peripheral nerves," *IEEE Trans. Biomed. Eng.*, vol. BME-33, no. 2, pp. 203–214, Feb. 1986.

[2] R. R. Riso, "Strategies for providing upper extremity amputees with tactile and hand position feedback—Moving closer to the bionic arm," *Technol. Health Care*, vol. 7, no. 6, pp. 401–409, Jan. 1999.

[3] R. L. Weiner and K. L. Reed, "Peripheral neurostimulation for control of intractable occipital neuralgia," *Neuromodulation*, vol. 2, no. 3, pp. 217–221, Jul. 1999.

[4] K. V. Slavin and K. J. Burchiel, "Use of long-term nerve stimulation with implanted electrodes in the treatment of intractable craniofacial pain," *J. Neurosurg.*, vol. 92, p. 576, 2000.

[5] L. W. Stinson, G. T. Roderer, N. E. Cross, and B. E. Davis, "Peripheral subcutaneous electrostimulation for control of intractable postoperative inguinal pain: A case report series," *Neuromodulation*, vol. 4, no. 3, pp. 99–104, 2001.

[6] R. M. Paicius, C. A. Bernstein, and C. Lempert-Cohen, "Peripheral nerve field stimulation for the treatment of chronic low back pain: Preliminary results of long term follow-up: A case series," *Neuromodulation*, vol. 10, no. 3, pp. 279–290, Jul. 2007.

[7] A. E. Yakovlev and A. T. Peterson, "Peripheral nerve stimulation in treatment of intractable postherpetic neuralgia," *Neuromodulation*, vol. 10, no. 4, pp. 373–375, Oct. 2007.

[8] B. Smith, P. H. Peckam, M. W. Keith, and D. D. Roscoe, "An externally powered, multichannel, implantable stimulator for versatile control of paralyzed muscle," *IEEE Trans. Biomed. Eng.*, vol. BME-34, pp. 499–508, Jul. 1987.

[9] S. Boyer, M. Sawan, M. A. Gawad, S. Robin, and M. M. Elhilali, "Implantable selective stimulator to improve bladder voiding: Design and chronic experiments in dogs," *IEEE Trans. Rehabil. Eng.*, vol. 8, no. 4, pp. 464–470, Dec. 2000.

[10] N. Xue, S. P. Chang, and J. B. Lee, "A SU-8-based compact implantable wireless pressure sensor for intraocular pressure sensing application," in *Proc. IEEE EMBC*, 2011, pp. 2854–2857.

[11] N. Xue, J. B. Lee, S. Foland, and S. P. Chang, "Biocompatible polymeric wireless pressure sensor for intraocular pressure sensing application," in *Proc. IEEE Sensors*, 2011, pp. 1748–1751.

[12] W. Mokwa and U. Schnakenberg, "Micro-transponder systems for medical applications," *IEEE Trans. Instrum. Meas.*, vol. 50, no. 6, pp. 1551–1555, Dec. 2001.

[13] T. Akin, K. Najafi, and R. M. Bradley, "A wireless implantable multichannel digital neural recording system for a micromachined sieve electrode," *IEEE J. Solid-State Circuits*, vol. 33, no. 1, pp. 109–118, Jan. 1998.

[14] C. W. Peng, J. J. J. Chena, C. C. K. Lin, P. W. F. Poon, C. K. Liang, and K. P. Lin, "High frequency block of selected axons using an implantable microstimulator," *J. Neurosci. Methods*, vol. 134, no. 1, pp. 81–90, Mar. 2004.

[15] L. S. Theogarajan, "A low-power fully implantable 15-channel retinal stimulator chip," *IEEE J. Solid-State Circuits*, vol. 43, no. 10, pp. 2322–2337, Oct. 2008.

[16] M. Ghovanloo and K. Najafi, "A wireless implantable multichannel microstimulating system-on-a-chip with modular architecture," *IEEE Trans. Neural Syst. Rehabil. Eng.*, vol. 15, no. 3, pp. 449–457, Sep. 2007.

[17] G. Voskerician, M. Shive, R. Shawgo, H. V. Recum, J. Anderson, M. Cima, and R. Langer, "Biocompatibility and biofouling of MEMS drug delivery devices," *Biomaterials*, vol. 24, no. 11, pp. 1959–1967, May 2003.

[18] S. H. Cho, H. M. Lu, L. Cauller, M. I. Romero-Ortega, J. B. Lee, and G. A. Hughes, "Biocompatible SU-8-based microprobes for recording neural spike signals from regenerated peripheral nerve fibers," *IEEE Sensors J.*, vol. 8, no. 11, pp. 1830–1836, Nov. 2008.

[19] S. H. Cho, L. Cauller, W. Rosellini, and J. B. Lee, "A MEMS-based fully-integrated wireless neurostimulator," in *Proc. IEEE MEMS*, Hong Kong, Jan. 2010, pp. 300–303.

[20] K. Finkenzeller, *RFID Handbook*. Hoboken, NJ: Wiley, 1999.

[21] N. Xue, S. H. Cho, S. P. Chang, and J. B. Lee, "Systematic analysis and experiment of inductive coupling and induced voltage for inductively coupled wireless implantable neurostimulator application," *J. Micromech. Microeng.*, vol. 22, no. 7, pp. 075008-1–075008-10, Jul. 2012.

[22] M. Ghovanloo, "Switched-capacitor based implantable low-power wireless microstimulating systems," in *Proc. IEEE Int. Symp. Circuits Syst.*, May 2006, pp. 2197–2200.
[23] D. R. Merrill, M. Bikson, and J. G. R. Jefferys, "Electrical stimulation of excitable tissue: Design of efficacious and safe protocols," *J. Neurosci. Methods*, vol. 141, no. 2, pp. 171–198, Feb. 2005.
[24] S. F. Cogan, "Neural stimulation and recording electrodes," *Annu. Rev. Biomed. Eng.*, vol. 10, pp. 275–309, Aug. 2008.

Sung-Hoon Cho received the B.S. degree in electrical engineering from Hanyang University, Seoul, Korea, in 2004, and the M.S. degree in electrical engineering and the Ph.D. degree from The University of Texas at Dallas (UT Dallas), Richardson, in 2006 and 2010, respectively.

In 2005, he was with the MEMS research group of the Micro–Nano Devices and Systems Laboratory, Department of Electrical Engineering, UT Dallas. His research interests were biological MEMS for peripheral nerve recording and stimulation, high-aspect-ratio three-dimensional on-chip inductors, and MEMS fabrication technologies. Since May 2010, he has been with Samsung Electronics Company, Ltd., Seoul, as a 32-nm high-k metal-gate Process Integration Engineer for the foundry business of the System Large Scale Integration Division.

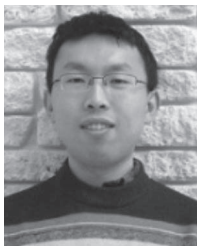

Ning Xue (S'11) received the B.S. and M.S. degrees in electrical engineering from Dalian University of Technology, Dalian, China, in 2005 and 2008, respectively, and the Ph.D. degree from The University of Texas at Dallas, Richardson, in 2012.

Since 2009, he has been with the MEMS research group of the Micro–Nano Devices and Systems Laboratory, Department of Electrical Engineering, The University of Texas at Dallas, Richardson. He is also currently a MEMS Development Engineer with Agiltron, Inc., Woburn, MA. His research interests include infrared detectors, neutron detectors, radiation detectors, MEMS fabrication, microfluidic devices, biological MEMS for wireless implantable application, pressure sensors, and RF MEMS systems.

Lawrence Cauller received the B.S. degree in psychology from The University of Utah, Salt Lake City, in 1980, the M.A. degree in psychology and neuroscience from Dalhousie University, Halifax, NS, Canada, in 1981, and the Ph.D. degree in biological sciences from the College of Medicine, Northeast Ohio Medical University, Rootstown, in 1988.

He was an Associate Professor with the Neuroscience Program, School of Behavioral and Brain Sciences, The University of Texas at Dallas, Richardson, from which he retired in 2011.

Will Rosellini, photograph and biography not available at the time of publication.

Jeong-Bong (JB) Lee (S'92–M'98–SM'08) received the B.S. degree in electronic engineering from Hanyang University, Seoul, Korea, in 1986, and the M.S. and Ph.D. degrees in electrical engineering from Georgia Institute of Technology, Atlanta, in 1993 and 1997, respectively.

In 2007, he was a Member of the External Review Panel for the Microsystems Division, Sandia National Laboratories. He is currently a Full Professor with the Department of Electrical Engineering, The University of Texas at Dallas, Richardson. His current research interests include MEMS and nanophotonics.

Dr. Lee was a recipient of a National Science Foundation Career Award in 2001. He served as an Executive Program Subcommittee member for the Transducers 2011 Conference and a Program Committee member for the IEEE Sensors Conference (2007–2009).